CrossMark

ORIGINAL RESEARCH

Enhancement of adsorption carbon capture capacity of 13X with optimal incorporation of carbon nanotubes

Naef A. A. Qasem[1] · Rached Ben-Mansour[1] · Mohamed A. Habib[1]

Abstract Carbon capture by physical adsorption can strongly participate in the reduction of the carbon dioxide emissions from the flue gases with minimum energy penalties. In this paper, we report the experimental data for enhancing the adsorption separation capability of zeolite 13X incorporated with carbon nanotubes (CNT). Six samples (13X, XC1, XC2, XC3, XC4, and XC5) have been characterized by XRD. Equilibrium adsorption isotherms and actual dynamic behavior of adsorption breakthrough tests were conducted. XRD analyses show that all the samples have almost identical XRD patterns to pure 13X, while the equilibrium isotherms indicate that XC3 (0.5 wt% CNT/13X) has CO_2 adsorbed amounts much closer to those of pristine 13X. Interesting results of actual capturing behavior were exposed during the breakthrough tests which confirm that the optimal adsorption separation is associated with XC3 with an increased adsorption capacity and separation breakpoint by about 21.4 and 25.3%, respectively, in comparison to pure 13X.

Keywords Adsorption · Zeolite 13X · CNT · Isotherms · Breakthrough · Carbon capture

List of symbols

C	Concentration (mol/m^3)
D	Diameter, size (m)
ΔH	Heat of adsorption (J/mol)
ε	Porosity
K_o	Toth adsorption constants (1/kPa)
K_{eq}	Toth adsorption constant (1/kPa)
n	Toth adsorption constant
q	Adsorption uptake (mmol/g)
Q_F	Feed volumetric flow rate at standard conditions (m^3/s^{-1})
P	Pressure (Pa)
R	Universal gas constant (J/mol K)
t	Time (s)
T	Temperature (K)
tss	Stoichiometric time (s)
y	Mole fraction

Subscript

CO_2, N_2	Carbon dioxide, nitrogen gas
ac	Actual conditions
p	Particle
i	Gas species index
g	Gas
s	Standard conditions
0	Inlet

Abbreviations

13X	Zeolite 13X
XC1	0.1 wt% CNT/13X
XC2	0.25 wt% CNT/13X
XC3	0.5 wt% CNT/13X
XC4	0.75 wt% CNT/13X
XC5	1.5 wt% CNT/13X
CNT	Carbon nanotubes

✉ Mohamed A. Habib
mahabib@kfupm.edu.sa

[1] Mechanical Engineering Department and KACST-TIC on CCS, King Fahd University of Petroleum and Minerals, Dhahran 31262, Saudi Arabia

Springer

Introduction

The greenhouse gases, including those emitted from combustion and industrial processes, such as carbon dioxide, nitrogen oxide, and methane, lead significantly to global warming, shore floods, atmospheric heat waves, land droughts, and destruction of cold-marine life. Moreover, the change in climate is expected to reduce the world's gross domestic product by about 5–20% [1]. The increase of the atmospheric temperature was about 0.74% in the last century and is predicted to reach about 6.4% at the end of this century [1]. This increase in temperature due to global warming/greenhouse effect leads to gross discomfort for inhabitants of the earth. In addition, huge amounts of sea and glaciers ice have being melt causing at least 0.2 mm rising in global sea level [2]. The most prevalent gas component of the greenhouse gases is carbon dioxide [3]. Therefore, the most of world environmental organizations are seriously requesting all industrial countries to minimize the emission of CO_2. The main source of CO_2 emission is considered to be the fossil fuel combustion processes, whereby the fossil fuel appears to be the most dominating source of electricity on a global scale and, therefore, plays a vital role for a comfortable and sustainable lifestyle. Therefore, the only currently available feasible solution to continue fossil fuel utilization to meet energy demands with minimized CO_2 emission is carbon capture and storage, with the secondary aim of mitigating the global climate change.

The on-going research in the field of carbon capture and storage (CCS) is gaining momentum every day. A vast majority of researchers have already investigated CO_2 separation and storage, using both experimental and simulation methods, with the primary objective of developing novel adsorption materials or adsorbents for this purpose [4]. The foremost advantage of using adsorption as a means of CO_2 separation is the ease of regeneration of the adsorbent material by applying heat and/or decreasing the operating pressure [5]. Activated carbons and zeolites are currently the most commonly exploited adsorbents in the context of research based on CO_2 separation and storage. More specifically, zeolites have been researched to a larger extent than activated carbons for carbon capture and hydrogen storage in applications involving relatively lower operating pressures [6, 7], whereas carbon-based materials, including activated carbons, have been preferred over zeolites for high pressure applications [7, 8]. However, the noticeable advantages of carbon-based materials over zeolite-based adsorbents include cost-effectiveness, stability towards exposure to water vapor, lower energy required for regeneration due to lower heat of adsorption, and ease

of production on a commercial scale [9]. A novel class of mesoporous materials have been discovered almost two decades ago which are referred to as metal-organic frameworks (MOFs) in accordance with an organic portion (linker) and an inorganic constituent (metal ion clusters) coexisting in the same structure [10]. In the context of CO_2 adsorption, MOF-2 appeared as the first candidate to be evaluated for CO_2 uptake as well as selectivity [10]. The highest CO_2 uptake was, however, reported for MOF-177 as 1470 mg/g at 35 bar [11]. In the subsequent years, a vast majority of MOFs have been synthesized by research communities worldwide with the aim of designing the most optimum framework topology to maximize the CO_2 uptake as well as selectivity simultaneously. More specifically, a total of about 54,341 MOFs designed for these applications have been recorded in the Cambridge Structure Database before July 2015 [12].

Only a few studies were conducted with the objective of improving CO_2 adsorption capacity of adsorbents via physical adding or chemical impregnating second-phase material (e.g., CNT) with the main adsorbents. For example, incorporating titanium with DMS-TN showed almost twice CO_2 adsorption capacity and more stability than those of pristine adsorbent (DMS-TN) [13]. In this context, the most studies used amine materials to be incorporated with some adsorbents in peruse of improving CO_2 uptake. Polyethylenimine (PEI)-impregnated millimeter-sized mesoporous carbon spheres have been developed and studied for improving CO_2 post-combustion capture [14]. The maximum CO_2 uptake was found to be about 163.4 mg/g at 0.15 bar and 75 °C. However, it was observed to decline during the cyclic adsorption/desorption experiment. A recent investigation aimed at improving the CO_2 uptake and separation efficiency of MIL-101(Cr) by incorporation of polyethyleneimine (PEI) in the framework resulting in PEI/MIL-101(Cr) composites. The results demonstrated a relatively lower adsorption capacity of CO_2 for PEI/MIL-101(Cr) composites compared to that measured for pristine MIL-101(Cr); however, the selectivity of CO_2 over N_2 was significantly improved [15]. Modification of 13X by impregnation with mono-ethanol amine (MEA) indicated to an improvement in the CO_2 adsorption capacity by a factor of ca. 1.6 at 30 °C, and that increased in the presence of moisture [16].

Since the last one and a half decade, carbon nanotubes (CNTs) have also attracted a considerable attention of research groups engaged in carbon capture and sequestration in view of the chemical affinity exhibited by CNTs towards CO_2 uptake and selectivity [17–21]. More specifically, the attachment of amino-functionalities to the

sidewalls of CNTs has resulted in a considerable enhancement in the intrinsic CO_2 adsorption capacity measured for CNTs [22–25]. Su et al. [26] studied the effect of functionalization of CNTs on the CO_2 uptake and selectivity for 3-aminopropyltriethoxysilane (APTES) groups. They found that the co-existence of moisture increased the CO_2 adsorption capacity measured for APTES-functionalized CNTs. The CO_2 adsorption capacity was measured to be about 2.59 mol/kg at 293 K for APTES-functionalized CNTs which clearly confirms functionalization to be an effective tool for improving the intrinsic CO_2 adsorption potential of CNTs. Adding CNT to an adsorbent can correspondingly enhance the thermal conductivity and then improves the adsorption capacity of adsorbents [27–29]. That is because the increase of the heat dissipation across the adsorbent bulk during adsorption process which cools down the adsorbent and then enhances CO_2 uptake. Moreover, increasing adsorbent effective thermal conductivity improves the heat transfer from a heat source to the adsorbent particles during desorption process and hence accelerates the CO_2 evacuation from adsorbents. For instance, the composite of CNT and $13X/CaCl_2$ showed higher thermal conductivity and adsorption capacity values than those of $13X/CaCl_2$ and pure 13X [27, 28]. More stability and adsorption capacity were also obtained with incorporating CNT with MIL101-68 (Al) [29]. In the same fashion, incorporating CNT and lithium ions with MOF $Cu_3(btc)_2$ resulted in improving the CO_2 capacity by about 305% comparing with the base adsorbent ($Cu_3(btc)_2$) [30].

The present research work aims at investigating the effect of physical mixing of 13X within small quantities of carbon nanotubes (less than 1.5 wt%), aiming at improving the thermal properties of adsorbent (e.g., thermal conductivity and heat capacity), with the end goal is to enhance the carbon dioxide adsorption capacity and separation behavior. To achieve this goal, experimental work, including measurement of equilibrium adsorption isotherms and XRD characterization of all samples, is required. In addition, the breakthrough separation tests are performed for determining the actual behavior of binary mixture of CO_2 and N_2 (20% v/v. and 80% v/v.) and for quantifying the level of improvements on CO_2 separation and capacity.

Experimental methods

Preparation of the samples

The samples were prepared by adding and mixing small quantities of carbon nanotube (CNT) into zeolite 13X. The utilized 13X, a commercial adsorbent imported from SORBEAD INDIA as molecular sieve pallets (1.5 mm size), was grinded to be an appropriate powder form for consistently mixing with CNT (multi walled). Six samples were made by adding different percentages of CNT (0, 0.1, 0.25, 0.5, 0.75, and 1.5% by weight) to 13X and named as: 13X, XC1, XC2, XC3, XC4, and XC5. The increase of CNT amounts makes the color of the composite darker, as shown in Fig. 1. The particle size distribution has also been measured using Particles-Size Analyzer Model S3500.

X-ray powder diffraction analysis

Powder X-ray diffraction patterns were obtained and collected using a Bruker D8-Advance Diffractometer (Cu K_α $\lambda = 1.54056$ Å) with an operating power of 30 kV/30 mA. The data were recorded by the step-counting method (step $= 0.02°$, time $= 3$ s) in the range $2\theta = 3°$–$45°$ at ambient temperature of 298 K.

Gas sorption measurements

Each sample (50–200 mg) was transferred to pre-weighted 9 mm large bulb glass sample cell and degassed at 200 °C under vacuum for 24 h on XeriPerp degasser (Quantachrome Instruments) which is equipped with a turbo molecular vacuum pump and controlled heat jackets. The gas sorption isotherms were collected on Autosorb and Quadrasorb adsorption instruments (Quantachrome Instruments). Apparent surface areas were obtained from nitrogen adsorption isotherms at 77 K (using Quadrasorb) as well as from carbon dioxide adsorption isotherms collected at 273 K (using Autosorb) by applying Brunauer–Emmett–Teller (BET) model. The average pore radius and pore volume were determined at 77 K for N_2 adsorption isotherms. Moreover, Autosorb was employed to collect N_2 and CO_2 adsorption isotherms at different temperatures (273 and 298 K). The determination of carbon dioxide heat

Fig. 1 Small samples of CNT/13X compounds

of adsorption (ΔH) was evaluated by applying the Clausius–Clapeyron expression for CO_2 isotherms at 273 and 298 K.

Binary gas (CO_2 + N_2) breakthrough experiments

The gas separation capabilities of all the samples were examined using a developed dynamic CO_2/N_2 breakthrough setup, as shown in Fig. 2. The system consists of a fixed adsorbent bed column (inner diameter = 9 mm, outer diameter = 13 mm and length = 20 cm) filled with CNT/13X compound (about 7 g), feed CO_2, and N_2 cylinders (for simulating a flue gas). The system included two gas regulators with dual pressure gauges and output control valves, two mass flow controllers (one was calibrated for CO_2 flow and the other was calibrated for N_2), two check valves (to control the flow in one direction), and a bypass line (for calibrating the mass spectrometer from the feed gas mixture). The system also comprised a bourdon absolute pressure, a mass spectrometer (to analyze the output concentration of effluent gases from the bed), heater jacket and vacuum pump (for desorption process to regenerate the adsorbent), and some valves and tubes to control the flow. All pipes and fittings were made of stainless steel to keep off corrosion contaminants. First, the samples were pretreated by heating at about 540 K under vacuum for 20 h to remove trapped gases and moisture inside the adsorbent. The experiments were performed at ambient conditions (297 K and 101.3 kPa). The mixed gas flow rate was 100 sccm (20% CO_2 and 80% N_2). The complete breakthrough of CO_2 and N_2 was indicated by the downstream gas composition reaching that of the feed gas. The carbon dioxide adsorption capacity (q_{CO_2}) is estimated using the following equation:

$$q_{CO_2} = \frac{\left(\frac{y_{CO_2} Q_F \text{tss} P_s}{RT_s} - \frac{y_{CO_2} V \varepsilon P_{ac}}{RT_{ac}} \right)}{m}, \tag{1}$$

where y_{CO_2} is the feed molar fraction of carbon dioxide, Q_F is the feed volumetric flow rate at standard conditions ($m^3 \ s^{-1}$), and V is the bed volume (m^3). P_s and T_s are the pressure and temperature at standard conditions (P in Pa and T in K). P_{ac} and T_{ac} are the pressure and temperature at actual conditions (P in Pa and T in K). R is the gas constant (8.314 J/mol K), ε is the total bed porosity, m is the mass of the adsorbent (kg), and tss is the stoichiometric time, which is integrated from the breakthrough curve using the following equation:

$$\text{tss} = \int_0^\infty \left(1 - \frac{c(t)}{c_0} \right) dt, \tag{2}$$

and $C(t)/C_0$ (C_{outlet}/C_{inlet}) is the concentration ratio of the outlet CO_2 concentration at specific time (t) over the inlet CO_2 concentration.

Results and discussion

To show the features of the physical mixture of CNT/13X compounds, we have captured some optical microscopic photos for all samples, as shown in Fig. 3. As evident, the CNT (black color) appears more as its percentage increases. Figure 4 shows the particle size distributions for all CNT/13X composites. They are close to each other for all the compounds; the majority of particles lay between 200 and 400 μm and between 800 and 1200 μm. The exception is that the XC4 composite has larger particle size distribution between 800 and 1400 μm. In addition, the particle distribution of

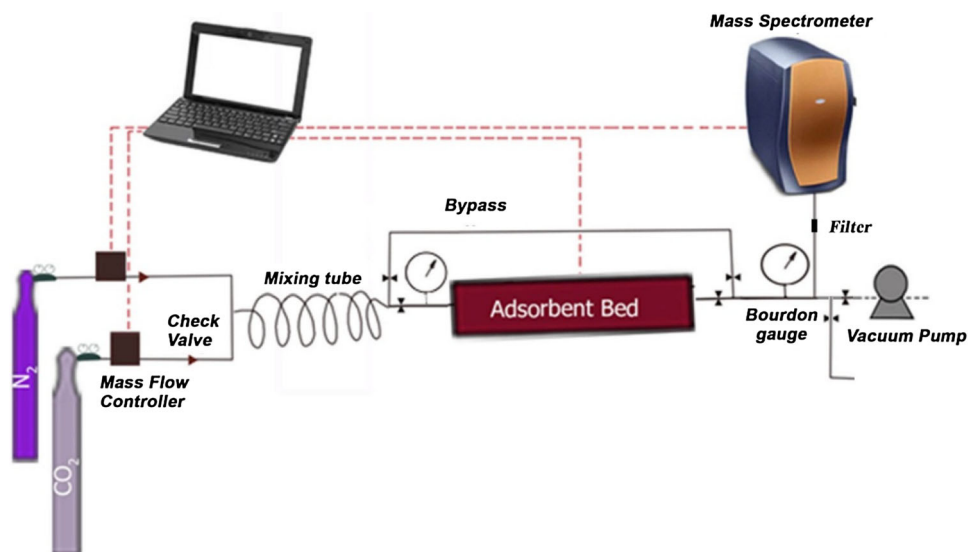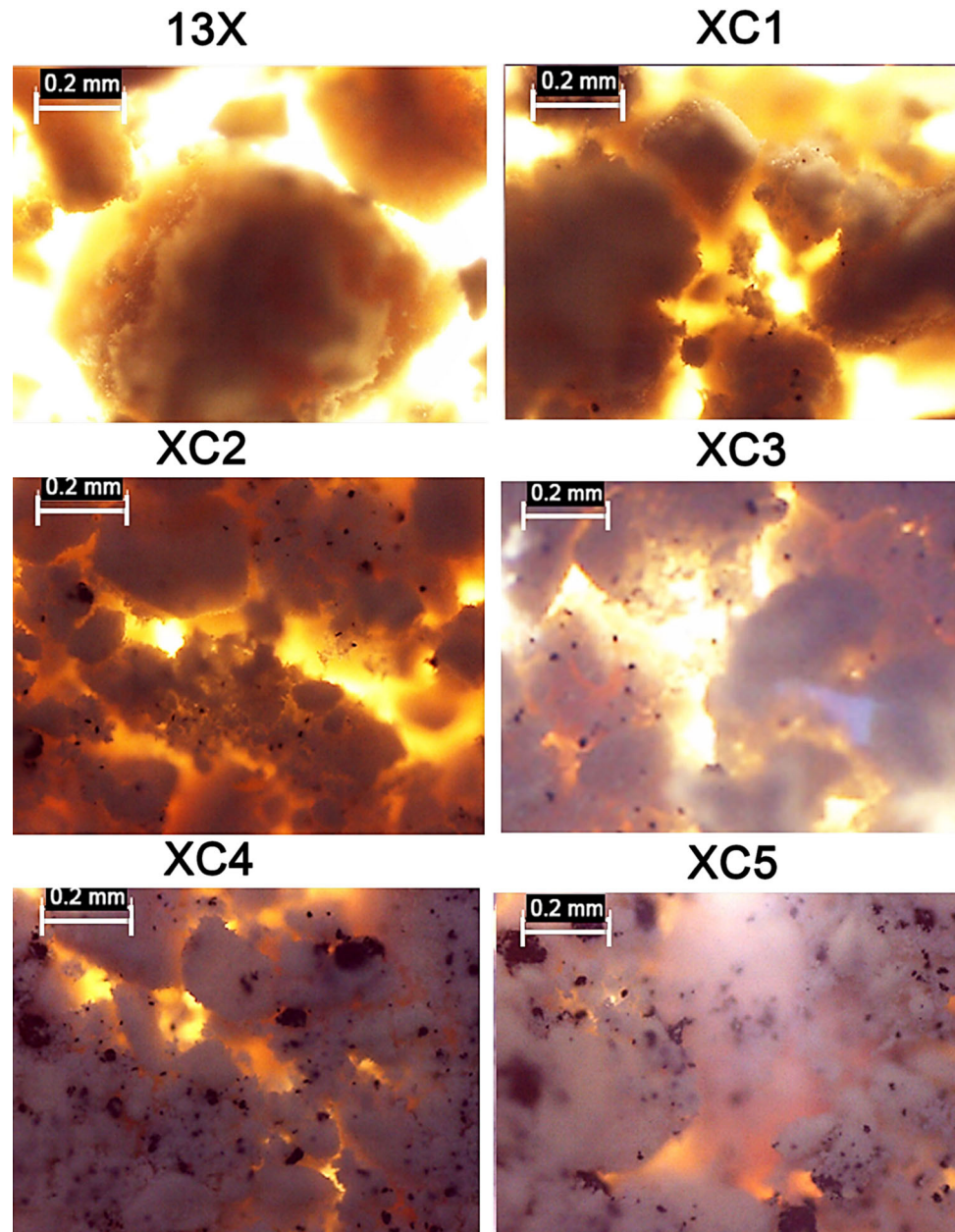Fig. 2 Schematic diagram of carbon dioxide adsorption capture breakthrough setup

Fig. 3 Optical microscopic photos of CNT/13X compounds

XC2 shows almost similar amounts of particles existing in the range of 1000–1400 μm. The similar distribution of the grain sizes is due to that the pure 13X pellets was grinded first, and then, all samples were composed by mixing the new powder of the pristine 13X with CNT. The grinding method could significantly control the grain size distribution. However, the large grain sizes can preferably be packed to the adsorbent bed with increasing the bed porosity and then minimizing the packing bed density. The high packed density could increase the pressure drop through the bed.

Powder X-ray diffraction analysis

Figure 5 illustrates the PXRD patterns of the seven samples (five of CNT/13X compounds and two of pure 13X and pure CNT). All the samples (excluded pure CNT) approximately show the same intensity peaks locations which are in good agreement with the pure 13X synthesized by Zheng et al. [31]. The error of intensity values is normal in such patterns due to a signal noise which could be generated from the sample thickness, powder distribution, sample position, orientation, XRD source, detector,

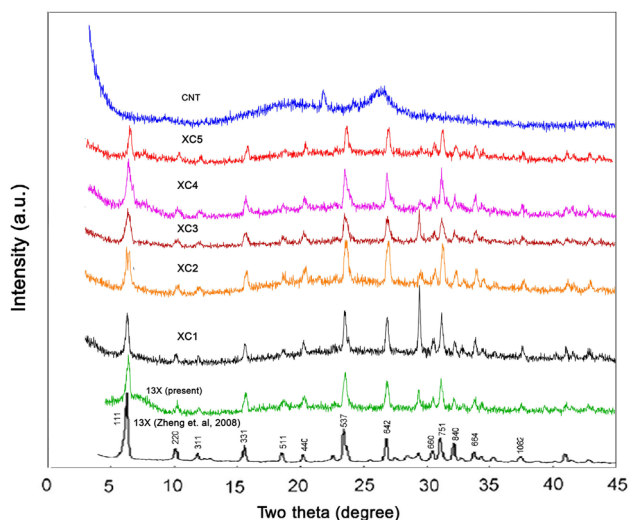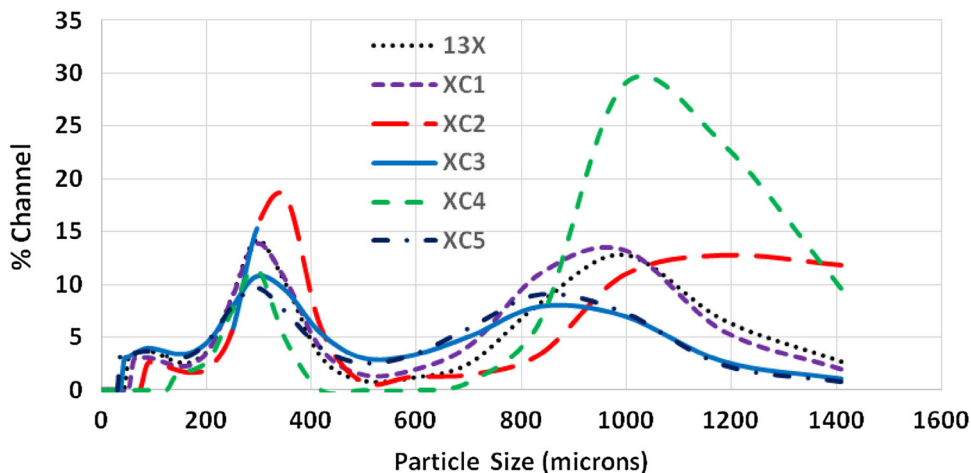**Fig. 4** Particle size distribution of CNT/13X compounds

Fig. 5 Powder X-ray diffraction (PXRD) data of CNT/13X compounds and pure materials (13X and CNT)

Fig. 6 N_2 adsorption isotherms of CNT/13X compounds at 77 K

Adsorption equilibrium isotherms of carbon dioxide and nitrogen

and so on. Therefore, the y-axis is always denoted by arbitrary unit (a.u.).

The peak appears at $2\theta = 28°$ with high values of intensity in some samples and small values in others (almost the peak is not clear for XC5) due to this noise. This peak is available in the samples that contain 13X, while it should not appear in CNT, because it (CNT) does not have any peak at this angle. The majority of the peaks of 13X are available in those of the all composite samples. To sum up, all the compound samples almost have the same structure of the pure 13X due to the small percentage of CNT added to the samples (less than 1.5% by weight), so the diffracted X-ray beam really emits from the crystalline cell's planes of 13X. The other reason is that the CNT has almost one or two small intensity peaks in the same range of operating angles ($2\theta = 3$–$45°$), as shown in Fig. 5.
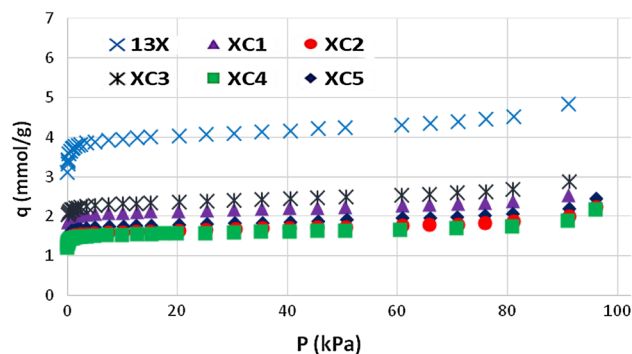
The adsorption isotherms of N_2 at 77 K are shown in Fig. 6. The tested samples exhibit sharp non-linear increasing for N_2 adsorbed amounts in the pressure range between 0 and 3 kPa followed by a steady increase of those amounts between 3 and 80 kPa and then the adsorbed N_2 values increased gradually at the end of the measured pressure (>80 kPa). 13X shows the highest equilibrium adsorption values. Then, the adsorbed values decline sharply by about 40% for XC3, which is still having better adsorption values than those of the remaining 13X/CNT compounds. Moreover, CO_2 adsorption isotherms are collected at 273 K, as shown in Fig. 7. The differences between CO_2 adsorbed amounts by pure 13X and XC3 are small compared with those of the others. Therefore, 13X and XC3 have the best adsorption equilibrium values under all applied pressure values (e.g., larger than 5 and 6.5 mmol/g could be adsorbed at $P = 20$ and 126 kPa, respectively). Table 1 summarizes BET surface areas (for
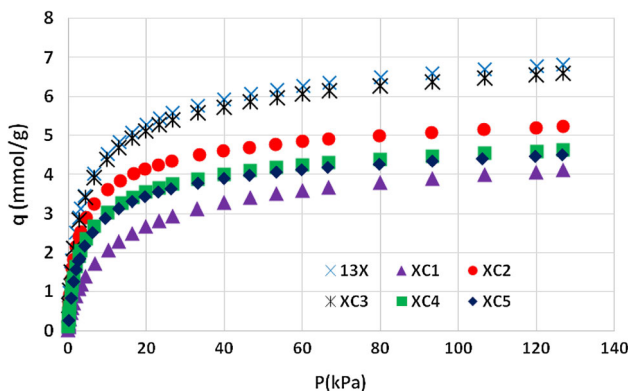
Fig. 7 CO_2 adsorption isotherms of CNT/13X compounds at 273 K

Fig. 8 N_2 adsorption isotherms of CNT/13X compounds at 298 K

N_2 at 77 K and CO_2 at 273 K), average pore size, and porous volume (for N_2 at 77 K) for all the samples.

The highest BET surface area is associated with 13X (about 1300 m²/g for N_2 and 573 m²/g for CO_2). The next highest BET is for XC3 (727 m²/g for N_2 and 552 m²/g for CO_2). In addition, the pore size is almost the same for the both cases (13X and XC3) by around 18.4 Å, while the other CNT/13X compounds have almost close values to each other by about 20.75 Å. In terms of the pore volume, the maximum value associates 13X (about 0.6 cc/g), whereas all CNT/13X compounds have a pore capacity of about 0.3 cc/g, which could be interpreted as the low-size CNT particles less than 13X pore size may easily penetrate inside the 13X macropores. It might be worth considering the closeness of adsorption properties (as SEM and gases uptake) of 13X and XC3 more than that of the other compounds is due to that they (13X and XC3) have the smallest pore radius (<9.2 Å) comparing to others (>10.1 Å). The smaller pore size, the greater surface area, and hence the higher adsorption capacity (under considering the pore characteristics effect and ignoring the effect of heat transfer characteristics).

The interesting adsorption isotherms have been collected for CO_2 and N_2 at ambient temperature (298 K), as shown in Figs. 8 and 9. Again, XC3 illustrates competitive adsorption values compared with pure 13X and better than the other CNT/13X mixtures. CO_2 adsorption values, generally, are more selective than N_2. For instance, CO_2 adsorbed amount is about 3.7 mmol/g for XC5 at $P = 1.2$
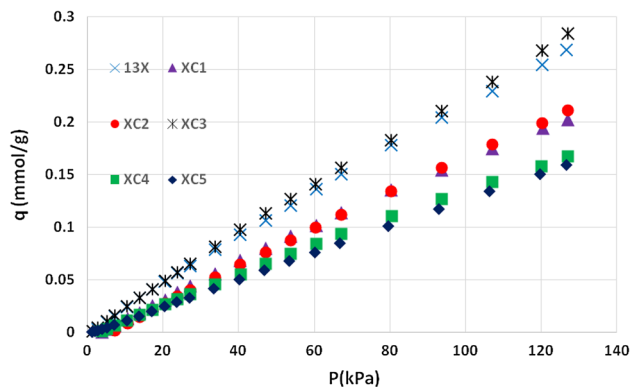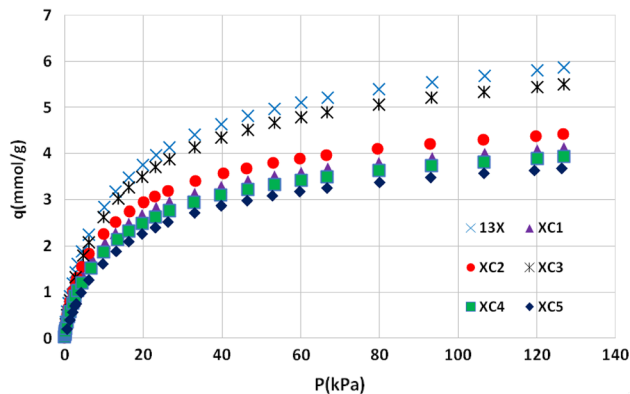

Fig. 9 CO_2 adsorption isotherms of CNT/13X compounds at 298 K
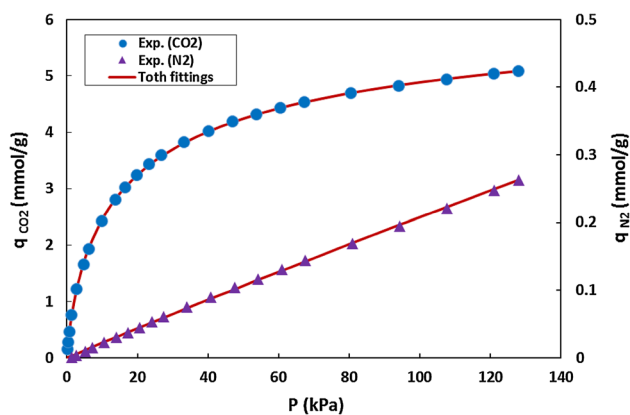

Fig. 10 Equilibrium isotherms and Toth fittings for XC3 at 298 K

Table 1 Pores characterization of the 13X incorporated with CNT

Characterizations	13X	XC1	XC2	XC3	XC4	XC5
BET (m²/g) @ 77 K for N_2	1304	685.24	575.34	727.04	528.1	519.46
BET (m²/g) @273 K for CO_2	573.75	385.2	364.58	552.07	381.02	378.46
Average pore radius (Å)	9.189	10.14	10.57	9.3	10.53	10.26
Pore volume (cc/g)	0.599	0.243	0.304	0.257	0.278	0.267

Table 2 Toth fitting parameters from experimental CO_2 and N_2 isotherms at 95% level of confidence

Parameter	Estimate	Lower limit	Upper limit
CO_2			
q_m (mmol/g)	6.6932	6.5597	6.8267
K_{eq} (1/kPa)	0.1385	0.1320	0.1451
n	0.5986	0.5788	0.6185
N_2			
q_m (mmol/g)	4.2247	−13.0054	21.4548
K_{eq} (1/kPa)	0.0005	−0.0016	0.0027
n	0.8738	−0.2137	1.9613

bars, while adsorbed quantity of N_2 at the same conditions is about 0.16 mmol/g. Consequently, 13X-based materials are considered as excellent materials for CO_2 separation from flue gases. Another advantage of 13X (with/without CNT) is an asymptotic trend of CO_2 adsorption values against the pressure, indicating that high adsorption values could be obtained at low pressure, such as a partial pressure of CO_2 in a flue gas (between 10 and 20%).

In pursuit of representing adsorption equilibrium isotherm results in the mathematical models, Toth fitting (Eq. 3) is satisfied. For example, Toth fitting for CO_2 and N_2 isotherms values of XC3 shows an excellent agreement with those of the experimental isotherms, as shown in Fig. 10. The important fitting parameters at 95% level of confidence are determined in Table 2.

$$q_i = \frac{q_{m,i}K_{eq,i}P_i}{[1 + (K_{eq,i}P_i)^{n_i}]^{1/n_i}}, \tag{3}$$

where q denotes to the equilibrium adsorption amount (mmol/g), and the subscript i is for CO_2 or N_2, q_m, K_{eq}, and n are the Toth fitting constants. q_m could be considered as the maximum adsorption capacity of the adsorbent, while K_{eq} could be later correlated to a function of a heat of adsorption (ΔH) and an operating temperature as formulated in the following equation:

$$K_{eq,i} = K_{0,i} \exp\left(\frac{\Delta H_i}{RT}\right) \tag{4}$$

where K_o is a constant (e.g., for $\Delta H_{CO_2} = 43,000$ J/mol, and then, $K_{0,CO_2} = 4.0176 \times 10^{-9}$ kPa^{-1}).

Figure 11 depicts the adsorption heat of CO_2 against the equilibrium adsorbed amounts for the all tested samples. The heat of adsorption is calculated using the Clausius–Clapeyron approach by the software associated with Autosorb (Quantachrome ASiQwin). The calculation of the heat of adsorption depends on the change of temperature and pressure at the same adsorbed values (q = constant), as shown in the following equation:
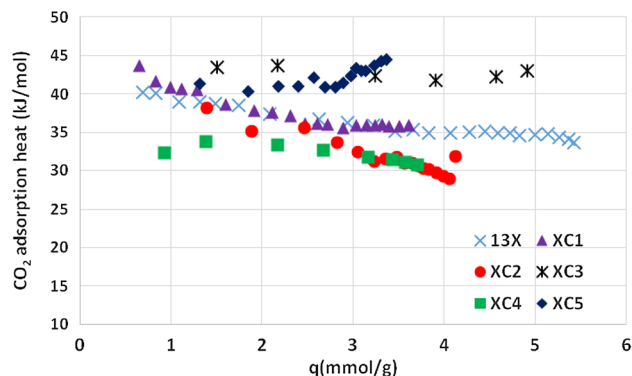
Fig. 11 CO_2 heat of adsorption (ΔH) for CNT/13X compounds

$$\Delta H = -R \left[\frac{d(\ln P)}{d\left(\frac{1}{T}\right)}\right]_{q=const}. \tag{5}$$

The adsorption heat values trends are almost linear against CO_2 adsorbed amounts, as shown in Fig. 11. The highest values of adsorption heat are obtained during adsorbing CO_2 by XC3 (ΔH(mean) = 42.8 kJ/mol), whereas 13X, XC1, XC2, XC4, and XC5 have average values of 36, 37.4, 31.9, 32.1, and 42.2 kJ/mol, respectively. These adsorption heats release during adsorption process causing increase in the adsorbent temperature. Moreover, these heats are needed during desorption processes, so the adsorbent temperature decreases during evacuation processes.

Experimental adsorption breakthrough of test CNT/13X compounds

To investigate the enhancements of the adsorption capacity and the carbon dioxide separation due to adding small amounts of CNT to the adsorbent (13X), breakthrough experiments are carried out. For this purpose, six samples of CNT/13X compounds have been put inside a stainless steel bed (length $L = 20$ cm, inner diameter $\emptyset = 9$ mm); the bed is tested in ambient temperature of 297 K and other conditions mentioned earlier.

The first records of breakthrough curves for CNT/13X composites are shown in Fig. 12. Indeed, there was a pressure drop may be caused by wrong packing. The pressure drops were monitored about 0.25, 0.38, 0.6, 0.7, and 0.75 bar, and the samples densities were 0.462, 0.501, 0.503, 0.502, and 0.459 g/cc for 13X, XC1, XC2, XC3, and XC4, respectively. As shown by the CO_2 isotherms, the CO_2 adsorbed amounts increase dramatically by increasing the pressure values, especially for the partial pressure of CO_2 below 30 kPa. This includes the breakthrough inlet pressure (P_{CO_2} is about 20 kPa at 0.2 molar fraction of the inlet pressure). Therefore, we tried to keep the same
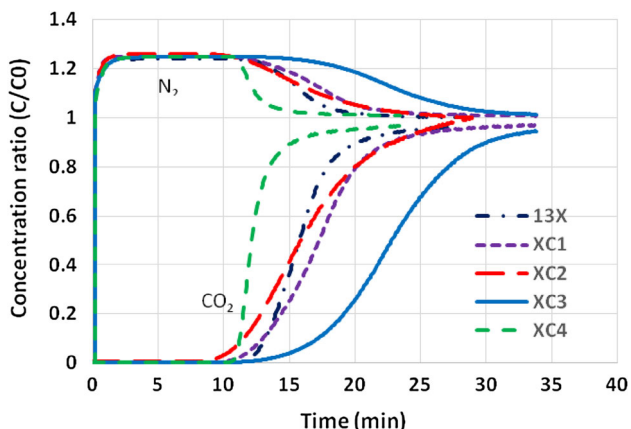
Fig. 12 CO_2 *breakthrough curves* of CNT/13X compounds at 297 K with variable packing density, noticeable pressure drop, and non-sufficient degasification process

operating condition for all the CNT/13X compounds. Moreover, the degassing process, before the adsorption process, was carried off at 423 K for 5 h which is not sufficient to evacuate the adsorbent from any guest gases. For these types of experimental errors, we cannot consider the breakthrough curves, shown in Fig. 12, sufficient to evaluate the effect of the incorporation of CNT with 13X. Therefore, we have repeated the experiments with new samples until reaching the most systematic one. In this case, the pressure drop is minimized to almost zero as optically observed by two bourdon gauges before and after the bed. The bed was filled with a constant packing density of about 0.553 cm^3 cc/g for all the CNT/13X compounds. The samples pre-treated by heating process have been elongated to be 20 h at about 540 K under vacuum. The curves of the systematic experimental adsorption breakthrough test are exhibited in Fig. 13. The breakthrough curves can clearly figure out the CO_2 adsorption period and adsorbed quantity (using Eq. 1) as well as the flow of N_2 through the bed. In these curves, the outlet concentration
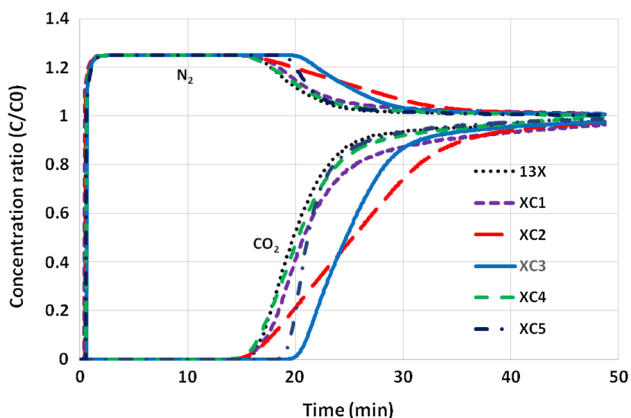
ratios of the both gases (CO_2/N_2) are plotted against the operating time. For each sample, the concentration ratio of CO_2 remains at zero at the bed outlet for the first 15–20 min (depends on the sample), while the concentration ratio values of N_2 rise up to about 1.25 due to the absence of CO_2 which is being adsorbed into the CNT/13X bed; the molar fraction of the CO_2 at outlet during adsorbing CO_2 period (<15–20 min) is zero, while it is 1 for N_2, and then, the concentration ratio C/C_0 (N_2) which mainly depends on the output/input molar fractions is about $1/0.8 = 1.25$. Eventually, the CO_2 concentration ratio increases up to 1 and decreases down to 1 that of N_2 after 15–20 min. It is noted from Fig. 13 that a breakpoint, a level at which the concentration ratio is less than 5% at the bed outlet, has an optimal value (about 21 min) for XC3 compound. This value is consecutively followed by that of XC5, XC1, XC2, and XC4. The breakpoints values are significant for a proper design period in the real applications to avoid emitting CO_2 to the atmosphere.

There is a noticeable variation of curves trends between breakpoints and saturation level, especially for XC2, XC3, and XC5; it is steeper for XC5, steady for XC2, and almost the same for 13X and XC3. This variation in the adsorption trends could be caused by many parameters such as particle size, diffusion resistances, or thermal resistances. In general, large particle size or/and small diffusion coefficient slow down the breakthrough trend. For 13X, XC2, XC3, and XC5, we have estimated the diffusion time constant $[D/rc^2$ (s^{-1}): D is the inter-particle diffusivity (m^2/s), and rc is the adsorbent crystal radius (m)] from CO_2 kinetic curves measured by dynamic vapor adsorption (DVS) for pressure range between 0 and 20 kPa and temperature of 298 K. The main results of the diffusion time constant and the average particle size are shown in Fig. 14. The value of the diffusion time constant of XC2 is higher than that of 13X which may indicate to higher CO_2 uptake being adsorbed by XC2, while the larger value of the average particle size could be responsible on the decline of XC2
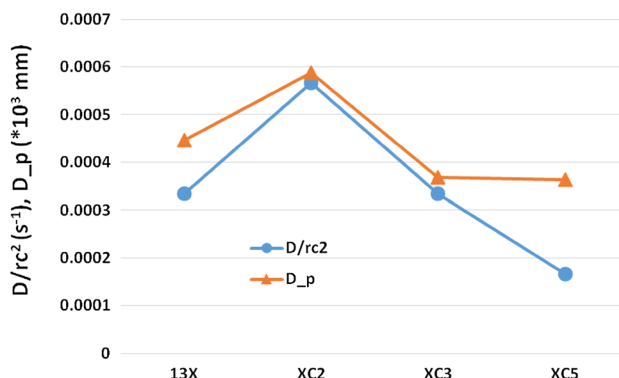

Fig. 13 CO_2 breakthrough curves of 13X-CNT compounds at 297 K and 101.3 kPa for the same amounts of adsorbents

Fig. 14 Average particle size (D_p) and diffusion time constant (D/rc^2) for 13X, XC2, XC3, and XC5
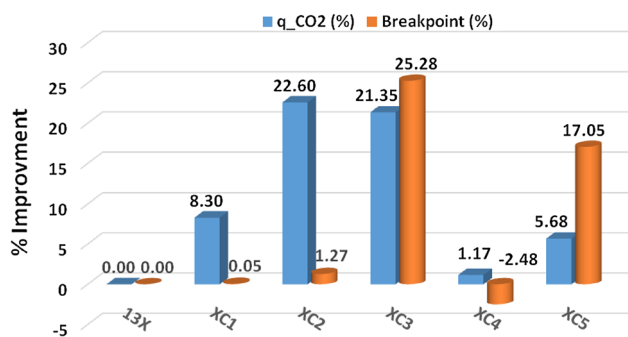
Fig. 15 Carbon dioxide adsorption capacity (*cubic bars*) and separation breakpoint (*cylindrical bars*) improvements (*percent*) for CNT/13X compounds at 297 K and 1.013 bars

Fig. 16 Measured effective heat capacities of CNT/13X compounds

breakthrough curve in compare with the trends of the other composites. For XC3, D/rc^2 has almost the same value of 13X, indicating that the diffusion properties is similar for both cases, while the little bit smaller particle sizes for XC3 could make the breakthrough curve slightly steeper. The change in adsorption capacity for 13X and XC3 might be referred to the change in the thermal resistances. The particle size of XC5 has the smallest values which could make the breakthrough curve steepest; however, the low value of the diffusion time was expected to slow the trend. It is clear that there are sometimes interferences between the effects of the particle size and the diffusion resistance on the breakthrough trends.

The calculated adsorbed amounts of CO_2 from experimental breakthrough curves using Eq. 1 are displayed in Fig. 15 as the ratio of improving the carbon dioxide adsorption capacity and separation breakpoint for all the CNT/13X compounds compared to the base sample (13X).

The improvement in the adsorption capacity values (Fig. 15) shows that the XC2 has an optimum value of 22.6% followed by about 21.6% for XC3. The carbon dioxide separation breakpoint enhancement gives all advantages to XC3 by about 25.3%. This value is followed by 17.1% associated with XC5. Consequently, XC3 has the resultant optimal values (adsorption capacity + adsorption breakpoint). It might be worth mentioning here that the higher value of the breakpoint, the greater value of adsorption heat, as shown in Figs. 11 and 15. This is attributed to a higher quantity of adsorbed CO_2 that
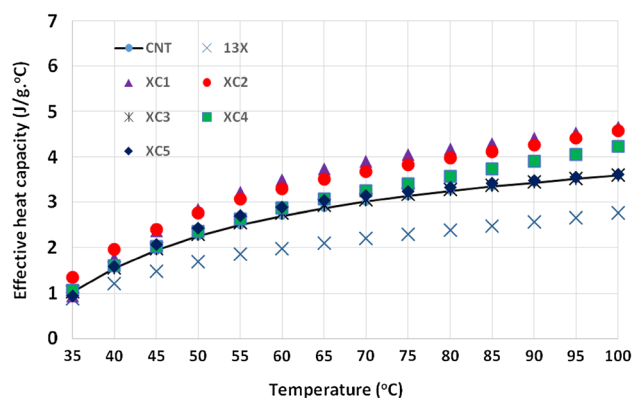
releases more heat during the adsorption process before appearing CO_2 in the outlet.

The present work shows a comparative CO_2 adsorption capacity comparing with some adsorbents reported in the literature as shown in Table 3.

It is also believed that the enhancement in the carbon dioxide adsorption capacity and separation has been caused by improving the thermal conductivity of 13X after adding CNT to 13X [27–29]. The thermal conductivity of CNT is considerably very high about 2000–5000 W/m K [35], so that the effective thermal conductivity of CNT/13X composites could be improved accordingly. Effective heat capacities, measured by differential scanning calorimeter (DSC, TA), show a quite considerable improvement after mixing with CNT as plotted in Fig. 16. It is noticed that the effective heat capacity values for all samples are higher than those of pure 13X in the temperature range between 35 and 100 °C.

Conclusion

The effect of adding carbon nanotubes to zeolite 13X on CO_2 adsorption separation and capacity has been investigated. Experimental methods have included XRD characterization, adsorption isotherms, and dynamic adsorption breakthrough. Six CNT/13X mixture samples are investigated: pure 13X, Xc1, XC2, XC3, XC4, and XC5. The equilibrium isotherms show that the adsorption quantities

Table 3 Dynamic CO_2 adsorption capacity of adsorbents

Adsorbent	Temperature (K)	CO_2 (vol%)	CO_2 capacity (mmol/g)	References
AC	301	20	0.734	[32]
MIL-101(Cr)	298	10	0.49	[33]
13X	301	20	2.35	[34]
13X	297	20	2.68	This work
XC2	297	20	3.29	This work
XC3	297	20	3.25	This work

for CO_2 and N_2 of XC3 (0.5 wt% CNT/13X) are close to those of pure 13X, while the other samples have lower adsorption values. XRD patterns have shown that all the samples have almost the same peaks as pure 13X due to less amounts of CNT added to the base adsorbent. The key results are represented by the breakthrough curves in which the optimal adsorption behavior of CO_2 separation and capacity (together) resulted from adding 0.5% by weight of CNT to 13X. The improvements are approximately 21.4% of the adsorption capacity and nearly 25.3% of the separation breakpoint compared to the base case (pure 13X).

References

1. Lee, S.-Y., Park, S.-J.: A review on solid adsorbents for carbon dioxide capture. J. Ind. Eng. Chem. **23**, 1–11 (2015)
2. Guardian: Antarctic-ship-stranding-delights-climate-change-sceptics (2014). http://www.theguardian.com. Accessed 1 Jan 2014
3. D'Alessandro, D.M., McDonald, T.: Toward carbon dioxide capture using nanoporous materials. Pure Appl. Chem. **83**(1), 57–66 (2010)
4. Ben-Mansour, R., Habib, M.A., Bamidele, O.E., Basha, M., Qasem, N.A.A., Peedikakkal, A., Laoui, T., Ali, M.: Carbon capture by physical adsorption: materials, experimental investigations and numerical modeling and simulations—a review. Appl. Energy **161**, 225–255 (2015)
5. Songolzadeh, M., Ravanchi, M.T., Soleimani, M.: Carbon dioxide capture and storage: a general review on adsorbents. World Acad. Sci. Eng. Technol. **70**, 225–232 (2012)
6. Choi, S., Drese, J.H., Jones, C.W.: Adsorbent materials for carbon dioxide capture from large anthropogenic point sources. ChemSusChem **2**(9), 796–854 (2009)
7. Siriwardane, R.V., Shen, M.-S., Fisher, E.P., Poston, J.A.: Adsorption of CO_2 on molecular sieves and activated carbon. Energy Fuels **15**(2), 279–284 (2001)
8. Mazumder, S., van Hemert, P., Busch, A., Wolf, K.H.A.A., Tejera-Cuesta, P.: Flue gas and pure CO_2 sorption properties of coal: a comparative study. Int. J. Coal Geol. **67**(4), 267–279 (2006)
9. Plaza, M.G., González, A.S., Pevida, C., Pis, J.J., Rubiera, F.: Valorisation of spent coffee grounds as CO_2 adsorbents for postcombustion capture applications. Appl. Energy **99**, 272–279 (2012)
10. Li, J.-R., Sculley, J., Zhou, H.-C.: Metal-organic frameworks for separations. Chem. Rev. **112**(2), 869–932 (2012)
11. Millward, A.R., Yaghi, O.M.: Metal-organic frameworks with exceptionally high capacity for storage of carbon dioxide at room temperature. J. Am. Chem. Soc. **127**(51), 17998–17999 (2005)
12. CCDC: Support Solution (2014). http://www.ccdc.cam.ac.uk. Accessed 1 May 2014
13. Zhang, X., Qin, H., Zhang, S., Wu, W.: Titanium-incorporated organic–inorganic hybrid adsorbent for improved CO_2 adsorption performance. Mater. Res. Bull. **62**, 200–205 (2015)
14. Wang, M., Yao, L., Wang, J., Zhang, Z., Qiao, W., Long, D., Ling, L.: Adsorption and regeneration study of polyethylenimine-impregnated millimeter-sized mesoporous carbon spheres for post-combustion CO_2 capture. Appl. Energy **168**, 282–290 (2016)
15. Lin, Y., Lin, H., Wang, H., Suo, Y., Li, B., Kong, C., Chen, L.: Enhanced selective CO_2 adsorption on polyamine/MIL-101(Cr) composites. J. Mater. Chem. A **2**(35), 14658–14665 (2014)
16. Hauchhum, L., Mahanta, P.: Carbon dioxide adsorption on zeolites and activated carbon by pressure swing adsorption in a fixed bed. Int. J. Energy Environ. Eng. **5**(4), 349–356 (2014)
17. Cinke, M., Li, J., Bauschlicher, C.W., Ricca, A., Meyyappan, M.: CO_2 adsorption in single-walled carbon nanotubes. Chem. Phys. Lett. **376**(5–6), 761–766 (2003)
18. Hsu, S.-C., Lu, C., Su, F., Zeng, W., Chen, W.: Thermodynamics and regeneration studies of CO_2 adsorption on multiwalled carbon nanotubes. Chem. Eng. Sci. **65**(4), 1354–1361 (2010)
19. Lithoxoos, G.P., Labropoulos, A., Peristeras, L.D., Kanellopoulos, N., Samios, J., Economou, I.G.: Adsorption of N_2, CH_4, CO and CO_2 gases in single walled carbon nanotubes: a combined experimental and Monte Carlo molecular simulation study. J. Supercrit. Fluids **55**(2), 510–523 (2010)
20. Su, F., Lu, C., Cnen, W., Bai, H., Hwang, J.F.: Capture of CO_2 from flue gas via multiwalled carbon nanotubes. Sci. Total Environ. **407**(8), 3017–3023 (2009)
21. Zhou, X., Yi, H., Tang, X., Deng, H., Liu, H.: Thermodynamics for the adsorption of SO_2, NO and CO_2 from flue gas on activated carbon fiber. Chem. Eng. J. **200–202**, 399–404 (2012)
22. Fatemi, S., Vesali-Naseh, M., Cyrus, M., Hashemi, J.: Improving CO_2/CH_4 adsorptive selectivity of carbon nanotubes by functionalization with nitrogen-containing groups. Chem. Eng. Res. Des. **89**(9), 1669–1675 (2011)
23. Gui, M.M., Yap, Y.X., Chai, S.-P., Mohamed, A.R.: Multi-walled carbon nanotubes modified with (3-aminopropyl)triethoxysilane for effective carbon dioxide adsorption. Int. J. Greenh. Gas Control **14**, 65–73 (2013)
24. Liu, Q., Shi, Y., Zheng, S., Ning, L., Ye, Q., Tao, M., He, Y.: Amine-functionalized low-cost industrial grade multi-walled carbon nanotubes for the capture of carbon dioxide. J. Energy Chem. **23**(1), 111–118 (2014)
25. Su, F., Lu, C., Chung, A.-J., Liao, C.-H.: CO_2 capture with amine-loaded carbon nanotubes via a dual-column temperature/vacuum swing adsorption. Appl. Energy **113**, 706–712 (2014)
26. Su, F., Lu, C., Chen, H.-S.: Adsorption, desorption, and thermodynamic studies of CO_2 with high-amine-loaded multiwalled carbon nanotubes. Langmuir **27**(13), 8090–8098 (2011)
27. Chan, K.C., Chao, C.Y.H., Wu, C.L.: Measurement of properties and performance prediction of the new MWCNT-embedded zeolite 13X/CaCl2 composite adsorbents. Int. J. Heat Mass Transf. **89**, 308–319 (2015)
28. Chan, K.C.C., Christopher Y.H.: Improved thermal conductivity of 13X/CaCl$_2$ composite adsorbent by CNT embedment. In: ASME Proceedings, Heat Transfer in Energy Systems, vol. 1, pp. HT2013–17168, V001T01A040 (2013)
29. Han, T., Xiao, Y., Tong, M., Huang, H., Liu, D., Wang, L., Zhong, C.: Synthesis of CNT@MIL-68(Al) composites with improved adsorption capacity for phenol in aqueous solution. Chem. Eng. J. **275**, 134–141 (2015)

30. Xiang, Z., Hu, Z., Cao, D., Yang, W., Lu, J., Han, B., Wang, W.: Metal-organic frameworks with incorporated carbon nanotubes: improving carbon dioxide and methane storage capacities by lithium doping. Angew. Chem. Int. Ed. **50**(2), 491–494 (2011)

31. Zheng, H., Han, L., Ma, H., Zheng, Y., Zhang, H., Liu, D., Liang, S.: Adsorption characteristics of ammonium ion by zeolite 13X. J. Hazard. Mater. **158**(2–3), 577–584 (2008)

32. Dantas, T.L.P., Luna, F.M.T., Silva, I.J., de Azevedo, D.C.S., Grande, C.A., Rodrigues, A.E., Moreira, R.F.P.M.: Carbon dioxide–nitrogen separation through adsorption on activated carbon in a fixed bed. Chem. Eng. J. **169**(1–3), 11–19 (2011)

33. Munusamy, K., Sethia, G., Patil, D.V., Somayajulu Rallapalli, P.B., Somani, R.S., Bajaj, H.C.: Sorption of carbon dioxide, methane, nitrogen and carbon monoxide on MIL-101(Cr): volumetric measurements and dynamic adsorption studies. Chem. Eng. J. **195–196**, 359–368 (2012)

34. Dantas, T.L.P., Luna, F.M.T., Silva Jr., I.J., Torres, A.E.B., de Azevedo, D.C.S., Rodrigues, A.E., Moreira, R.F.P.M.: Modeling of the fixed-bed adsorption of carbon dioxide and a carbon dioxide–nitrogen mixture on zeolite 13X. Braz. J. Chem. Eng. **28**(3), 533–544 (2011)

35. Han, Z., Fina, A.: Thermal conductivity of carbon nanotubes and their polymer nanocomposites: a review. Prog. Polym. Sci. **36**(7), 914–944 (2011)